

Electromagnetic, weak, and strong interactions of light mesons

P. Maris

Dept. of Physics, North Carolina State University, Raleigh, NC 27695-8202, U.S.A.

(Received: November 11, 2018)

The ladder-rainbow truncation of the set of Dyson–Schwinger equations is used to study a variety of electroweak and strong processes involving light mesons. The parameters in the effective interaction are constrained by the chiral condensate and f_π ; the current quark masses are fitted to m_π and m_K . The obtained electromagnetic form factors are in good agreement with the data. Also the weak K_{l3} decay and the radiative and strong decays of the vector mesons agree reasonably well with the data. Finally, we indicate how processes such as π - π scattering can be described within this framework as well.

1 Introduction

Our goal is to describe the hadrons and their interactions in terms of their constituents, quarks and gluons, using the underlying theory, QCD. The set of Dyson–Schwinger equations [DSEs] form a useful tool for this purpose [1]. In rainbow-ladder truncation, they have been successfully applied to calculate the masses and decay constants of light pseudoscalar and vector mesons [2, 3]. The dressed-quark propagator, as obtained from its DSE, together with the meson Bethe–Salpeter amplitude [BSA], form the necessary elements for calculations of strong interactions in impulse approximation, such as the $\rho \rightarrow \pi\pi$ decay. For electroweak processes, such as the electromagnetic form factors, radiative decays, and semileptonic decays, one also needs the $q\bar{q}\gamma$ and $q\bar{q}W$ vertices.

1.1 Dyson–Schwinger equations

The DSE for the renormalized quark propagator in Euclidean space is

$$S(p)^{-1} = i Z_2 \not{p} + Z_4 m(\mu) + Z_1 \int \frac{d^4 q}{(2\pi)^4} g^2 D_{\mu\nu}(p-q) \frac{\lambda^i}{2} \gamma_\mu S(q) \Gamma_\nu^i(q, p), \quad (1)$$

where $D_{\mu\nu}(k)$ is the dressed-gluon propagator and $\Gamma_\nu^i(q; p)$ the dressed-quark-gluon vertex. The most general solution of Eq. (1) has the form $S(p)^{-1} = i\not{p}A(p^2) + B(p^2)$ and is renormalized at spacelike μ^2 according to $A(\mu^2) = 1$ and $B(\mu^2) = m(\mu)$ with $m(\mu)$ the current quark mass.

Mesons are described by solutions of the homogeneous BSE

$$\Gamma_H(p_+, p_-; Q) = \int \frac{d^4 q}{(2\pi)^4} K(p, q; Q) S(q_+) \Gamma_H(q_+, q_-; Q) S(q_-), \quad (2)$$

at discrete values of $Q^2 = -m_H^2$, where m_H is the meson mass. In this equation, $p_+ = p + \eta Q$ and $p_- = p - (1 - \eta)Q$ are the outgoing and incoming quark momenta respectively, and similarly for q_\pm . The kernel K is the renormalized, amputated $q\bar{q}$ scattering kernel that is irreducible with respect to a pair of $q\bar{q}$ lines. Together with the canonical normalization condition for $q\bar{q}$ bound states, Eq. (2) completely determines the bound state BSA Γ_H . Different types of mesons, such as (pseudo-)scalar, (axial-)vector, and tensor mesons, are characterized by different Dirac structures.

The dressed $q\bar{q}\gamma$ and $q\bar{q}W$ vertices satisfy an inhomogeneous BSE: e.g. the quark-photon vertex $\Gamma_\mu(p_+, p_-; Q)$, with Q the photon momentum and p_\pm the quark momenta, satisfies [4]

$$\Gamma_\mu(p_+, p_-; Q) = Z_2 \gamma_\mu + \int \frac{d^4 q}{(2\pi)^4} K(p, q; Q) S(q_+) \Gamma_\mu(q_+, q_-; Q) S(q_-). \quad (3)$$

Solutions of the homogeneous version of Eq. (3) define vector meson bound states at timelike photon momenta $Q^2 = -m_V^2$. It follows that $\Gamma_\mu(p_+, p_-)$ has poles at those locations [5].

Table 1: Overview of results for the light pseudoscalar and vector meson masses and leptonic decay constants, all in GeV. Experimental data are from Ref. [6].

	m_π	f_π	m_K	f_K	m_ρ	f_ρ	m_{K^*}	f_{K^*}	m_ϕ	f_ϕ
calc.	0.138	0.131	0.497	0.155	0.742	0.207	0.936	0.241	1.072	0.259
expt.	0.138	0.131	0.496	0.160	0.770	0.216	0.892	0.225	1.020	0.236

1.2 Model truncation

To solve the BSE, we use a ladder truncation,

$$K(p, q; P) \rightarrow -\mathcal{G}((p - q)^2) D_{\mu\nu}^{\text{free}}(p - q) \frac{\lambda^i}{2} \gamma_\mu \otimes \frac{\lambda^i}{2} \gamma_\nu, \quad (4)$$

in conjunction with the rainbow truncation for the quark DSE: $\Gamma_\nu^i(q, p) \rightarrow \gamma_\nu \lambda^i / 2$ together with $Z_1 g^2 D_{\mu\nu}(k) \rightarrow \mathcal{G}(k^2) D_{\mu\nu}^{\text{free}}(k)$ in Eq. (1). This truncation preserves, independent of the details of the effective interaction $\mathcal{G}(k^2)$, both the vector Ward–Takahashi identity [WTI] for the $q\bar{q}\gamma$ vertex and the axial-vector WTI. The latter ensures the existence of massless pseudoscalar mesons connected with dynamical chiral symmetry breaking [2]. In combination with impulse approximation, the former ensures electromagnetic current conservation [5].

For the effective quark-antiquark interaction, we employ the Ansatz given in Ref. [3]. The ultraviolet behavior of this effective interaction is chosen to be that of the QCD running coupling $\alpha(k^2)$; the ladder-rainbow truncation then generates the correct perturbative QCD structure of the DSE-BSE system of equations. In the infrared region, the interaction is sufficiently strong to produce a realistic value for the chiral condensate of about $(240 \text{ GeV})^3$. With this model, we can solve the BSE for pseudoscalar and vector mesons, and calculate the meson masses and leptonic decay constants. The model parameters, along with the quark masses, are fitted to give a good description of the chiral condensate, $m_{\pi/K}$ and f_π . The results of our model calculations [3] are shown in Table 1 and are in reasonable agreement with the data.

2 Meson interactions

In impulse approximation, processes such as electromagnetic scattering, the weak K_{l3} decay, radiative and strong decays of vector mesons, can all be described by the same generic loop integral

$$I^{abc}(P, Q, K) = N_c \int \frac{d^4 q}{(2\pi)^4} \text{Tr} [S^a(q) \Gamma^{a\bar{b}}(q, q'; P) S^b(q') \Gamma^{b\bar{c}}(q', q''; Q) S^c(q'') \Gamma^{c\bar{a}}(q'', q; K)], \quad (5)$$

where $q - q' = P$, $q' - q'' = Q$, $q'' - q = K$, and momentum conservation dictates $P + Q + K = 0$. In Eq. (5), S^i is the dressed quark propagator with flavor index i , and $\Gamma^{i\bar{j}}(k, k'; P)$ stands for a generic vertex function with incoming quark flavor j and momentum k' , and outgoing quark flavor i and momentum k . Depending on the specific process under consideration, this vertex function could be a meson BSA, a $q\bar{q}\gamma$ vertex, or, in case of weak processes, a $q\bar{q}W$ vertex. In the calculations discussed below, the propagators, the meson BSAs, and the $q\bar{q}\gamma$ and $q\bar{q}W$ vertices are all obtained as solutions of their respective DSE in rainbow-ladder truncation, without adjusting any of the model parameters.

2.1 Electromagnetic form factors

Meson electromagnetic form factors in impulse approximation are described by two diagrams, with the photon coupled to the quark and to the antiquark respectively. Each diagram corresponds

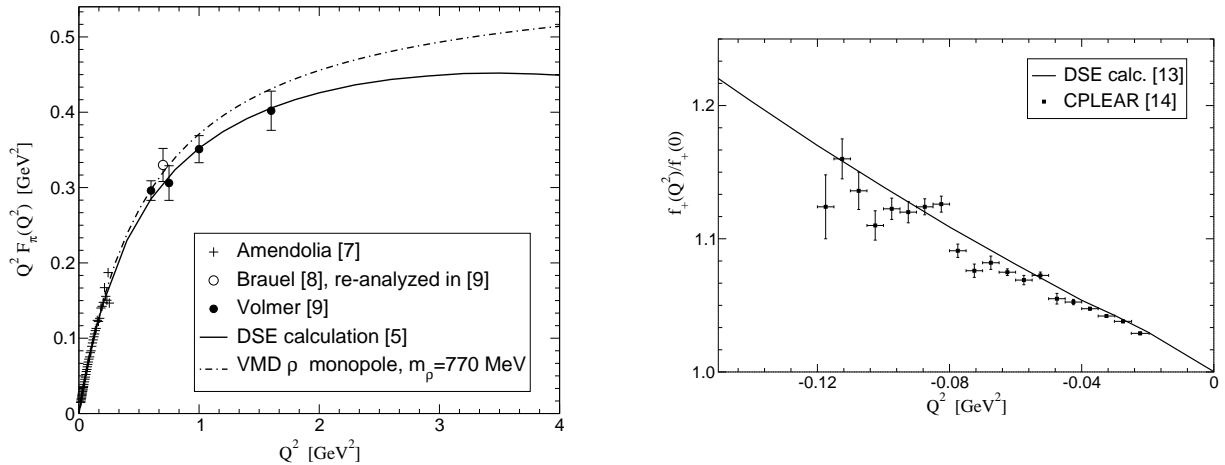


Figure 1: On the left, our result for $Q^2 F_\pi(Q^2)$, and right, our curve for the K_{l3} form factor $f_+(Q^2)$.

to an integral like Eq. (5) with two meson BSAs and one $q\bar{q}\gamma$ -vertex. With Q being the photon momentum, and the incoming and outgoing pseudoscalar mesons having momentum $P \mp Q/2$, we can define a form factor for each of these diagrams [5]

$$2 P_\nu F_{a\bar{b}\bar{b}}(Q^2) = I_\nu^{ab\bar{b}}(P - Q/2, Q, -(P + Q/2)). \quad (6)$$

We work in the isospin symmetry limit, and thus $F_\pi(Q^2) = F_{u\bar{u}u}(Q^2)$. The K^+ and K^0 form factors are given by $F_{K^+} = \frac{2}{3}F_{u\bar{s}u} + \frac{1}{3}F_{u\bar{s}\bar{s}}$ and $F_{K^0} = -\frac{1}{3}F_{d\bar{s}d} + \frac{1}{3}F_{d\bar{s}\bar{s}}$ respectively.

Our result for $Q^2 F_\pi$ is shown in Fig. 1, together with experimental data from Refs. [7–9]; the corresponding charge radius, together with the neutral and charged kaon charge radii, are given in Table 2. The obtained charge radii agree quite well with the experimental data [7, 10, 11], as do our form factors. Up to about $Q^2 = 2 \text{ GeV}^2$, our result for F_π can be described very well by a monopole with mass scale given by our calculated m_ρ , $m = 742 \text{ MeV}$. Above this value, our curve starts to deviate more and more from this naive VMD monopole. Our results for F_K are given in Ref. [5] and can be fitted quite well up to about $Q^2 = 2 \sim 3 \text{ GeV}^2$ by a monopole with mass scale slightly larger than the ρ mass. Asymptotically, these form factors behave like $Q^2 F(Q^2) \rightarrow c$ up to logarithmic corrections [12]. However, numerical limitations prevent us from accurately determining the constants c .

2.2 Weak interactions

The matrix element $\langle \pi^-(P + Q/2) | \bar{s}\gamma_\mu u | K^0(P - Q/2) \rangle$ describing the semileptonic decay of neutral kaons via a W -boson with momentum Q can be characterized by two form factors

$$I_\mu^{dsu}(P - Q/2, Q, -(P + Q/2)) = 2 P_\mu f_+(Q^2) + Q_\mu f_-(Q^2). \quad (7)$$

Table 2: Calculated charge radii in fm^2 , with expt. data [7, 10, 11], and K_{l3} observables. The double entries for the expt. K_{l3} data [6] correspond to the neutral and charged K_{l3} decays respectively.

	r_π^2	$r_{K^+}^2$	$r_{K^0}^2$	λ_+	λ_0	$-\xi$	$\Gamma(K_{e3})$	$\Gamma(K_{\mu3})$
calc.	0.45	0.38	-0.086	0.027	0.018	0.11	$7.38 \cdot 10^6 \text{ s}^{-1}$	$4.90 \cdot 10^6 \text{ s}^{-1}$
expt.	0.44	0.34	-0.054	.0276, .0288	.006, .025	0.31, 0.11	7.50, 3.89	5.26, 2.57

The form factors f_{\pm} for the K^0 decay are essentially the same as those for K^+ ; in the isospin limit, the only difference between the matrix elements for the K^0 and the K^+ decay is a factor of $\sqrt{2}$, the π^0 being $(u\bar{u} - d\bar{d})/\sqrt{2}$, which results in a factor of 2 difference in the partial decay width.

In the right panel of Fig. 1 we show our result for $f_+(t)$ [13], together with the experimental data for this form factor [14]. Experiments are often characterized in terms of the transverse, f_+ , and the scalar form factor f_0 , rather than f_- , which is defined by

$$f_0(Q^2) = \frac{Q_{\mu} I_{\mu}^{dsu}(P - Q/2, Q, -(P + Q/2))}{m_K^2 - m_{\pi}^2} = f_+(Q^2) - \frac{Q^2}{m_K^2 - m_{\pi}^2} f_-(Q^2). \quad (8)$$

The dimensionless slope parameter λ for these form factors is defined as $\lambda = -m_{\pi}^2 f'(0)/f(0)$; ξ is defined as $f_-(0)/f_+(0)$. The partial decay width can be obtained by integrating the decay rate, which depends on the lepton masses. Both the shape and the magnitude we obtain for these form factors agree well with experiments, as can be seen from Table 2.

2.3 Radiative decay of vector mesons

We can describe the radiative decay of the vector mesons using the same loop integral, Eq. (5), this time with one vector meson BSA, one pseudoscalar BSA, and one $q\bar{q}\gamma$ -vertex [18]. The on-shell value gives us the coupling constant, which can be used to calculate the partial decay width. For virtual photons, we can define a form factor $F_{VP\gamma}(Q^2)$, normalized to 1 at $Q^2 = 0$, which can be used in estimating meson-exchange contributions to hadronic processes [15–17].

In the isospin limit, the $\rho^0 \pi^0 \gamma$ and $\rho^{\pm} \pi^{\pm} \gamma$ vertices are identical, and are given by

$$\frac{1}{3} I_{\mu\nu}^{uuu}(P, Q, -(P + Q)) = \frac{g_{\rho\pi\gamma}}{m_{\rho}} \epsilon_{\mu\nu\alpha\beta} P_{\alpha} Q_{\beta} F_{\rho\pi\gamma}(Q^2), \quad (9)$$

where P is the ρ momentum. The $\omega \pi \gamma$ vertex is a factor of 3 larger, due to the difference in isospin factors. For the $K^* \rightarrow K\gamma$ decay, we have to add two terms: one with the photon coupled to the \bar{s} -quark and one with the photon coupled to the u - or d -quark, corresponding to the charged or neutral K^* decay respectively.

As Eq. (9) shows, it is $g_{VP\gamma}/m_V$ that is the natural outcome of our calculations; therefore, it is this combination that we report in Table 3, together with the corresponding decay widths [18]. The agreement between theory and experiment for $g_{VP\gamma}/m_V$ is within about 10%, except for the discrepancy in the charged $K^* \rightarrow K\gamma$ decay for which we have no explanation. Likewise the large difference between the neutral and charged ρ decay width is beyond the reach of the isospin symmetric impulse approximation. Note that part of the difference between the experimental and calculated decay width comes from the phase space factor because our calculated vector meson masses deviate up to 5% from the physical masses.

2.4 Strong decays of vector mesons

If we continue the calculation of the electromagnetic form factors into the timelike region, we find a pole at the mass of the vector meson bound states. Using the behavior of the electromagnetic form

Table 3: Vector meson radiative decays: coupling g/m in GeV^{-1} and partial decay width in keV.

	g/m	$\Gamma_{\rho^{\pm}\pi^{\pm}\gamma}$	$\Gamma_{\rho^0\pi^0\gamma}$	g/m	$\Gamma_{\omega\pi\gamma}$	g/m	$\Gamma_{K^{*\pm}K^{\pm}\gamma}$	g/m	$\Gamma_{K^{*0}K^0\gamma}$
calc.	0.69	53	(53)	2.07	479	0.99	90	1.19	130
expt.	0.74	68	(102)	2.31	717	0.83	50.3	1.28	116

Table 4: Overview of our results for vector meson strong decays (left): dimensionless coupling constants and partial decay width in MeV, and right, π - π scattering lengths, compared to leading order chiral perturbation theory, $a_0^0 = 7m_\pi^2/(8\pi f_\pi^2)$ and $a_0^2 = -m_\pi^2/(4\pi f_\pi^2)$ [20] (Weinberg's limit).

	$g_{\rho\pi\pi}$	$\Gamma_{\rho\pi\pi}$	$g_{\phi KK}$	$\Gamma_{\phi KK}$	$g_{K^*K\pi}$	$\Gamma_{K^*K\pi}$		a_0^0	a_0^2
calc.	5.4	115	4.3	6.7	4.0	31	calc.	0.170	0.045
expt.	6.02	151	4.64	2.2	4.60	50	Ref. [20]	0.156	0.045

factors $F_{u\bar{u}u}$ and $F_{u\bar{s}\bar{s}}$ around this pole, we can extract the coupling constants $g_{\rho\pi^+\pi^-}$ and $g_{\phi K^+K^-}$ respectively [18], which govern the strong decays $\rho \rightarrow \pi\pi$ and $\phi \rightarrow KK$. The results from this analysis are given in Table 4, and are reasonably close to the experimental data. Similarly, the two form factors f_+ and f_0 describing the weak K_{l3} decay exhibit poles at $Q^2 = -m_{K^*}^2$ and $Q^2 = -m_\kappa^2$ respectively, due to vector and scalar $u\bar{s}$ bound states [13]. From the behavior close to the pole we can extract the coupling constant for the strong decay $K^* \rightarrow K\pi$ as well. A direct calculation of the strong vector meson decays, using on-shell meson BSAs but different numerical techniques [19], agrees reasonably well with these results extracted from the electroweak form factors. Note that the factor of three difference between the experimental and our calculated decay width for the ϕ is due to the phase factor $(1 - 4m_K^2/m_\phi^2)^{3/2}$: with our calculated masses, this factor is 0.051, whereas with the actual physical masses this factor is 0.015. The dimensionless coupling constants agree within 10% to 15% with the experimental data.

3 π - π scattering

Although impulse approximation seems to work remarkably well for a variety of interactions involving three external particles, one has to go beyond impulse approximation in order to describe processes with four (or more) external particles. As an example, consider π - π scattering at threshold. The generic loop integral for π - π scattering in impulse approximation is

$$A = N_c \int \frac{d^4q}{(2\pi)^4} \text{Tr}[S(q)\Gamma_\pi(q, q')S(q')\Gamma_\pi(q', q'')S(q'')\Gamma_\pi(q'', q''')S(q''')\Gamma_\pi(q''', q)]. \quad (10)$$

At threshold in the chiral limit, $\Gamma_\pi(k + P/2, k - P/2) \rightarrow i\gamma_5 B(k^2)/f_\pi$, and thus

$$A \rightarrow 4N_c \int \frac{d^4k}{(2\pi)^4} \frac{B^4(k)/f_\pi^4}{(k^2 A^2(k) + B^2(k))^2}, \quad (11)$$

which is nonzero. On the other hand, chiral symmetry dictates that the threshold scattering amplitudes vanish in the chiral limit like m_π^2/f_π^2 [20]. Clearly, impulse approximation is insufficient to describe π - π scattering.

In order to properly describe π - π scattering in the rainbow-ladder truncation, all possible diagrams with one or more insertions of the ladder kernel K across two pion BSAs should be added to the impulse contribution [21], as indicated in Fig. 2. If we include these sets of ladder diagrams, we can show numerically that the threshold π - π scattering amplitudes indeed vanish like m_π^2/f_π^2 , using the same model as in the previous section. The corresponding scattering lengths are given in Table 4. We expect that in particular a_0^0 will receive significant corrections from pion loop effects, which we have not included in our calculation: in chiral perturbation theory, higher order corrections (i.e. pion loops) change the leading order result to $a_0^0 = 0.220$ and $a_0^2 = 0.0444$ [22].

So far, we have only considered π - π scattering, but also in other hadronic 4-particle processes one should consider the contributions from these infinite sums of ladder terms, in addition to

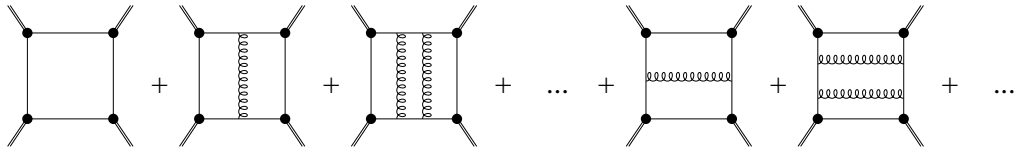


Figure 2: Diagrams needed to correctly describe π - π scattering in rainbow-ladder truncation [21].

the impulse term. In general, we expect the role of these summed ladder contributions to be less important than in π - π scattering, except for processes that receive significant contributions from resonances. By adding these ladder diagrams one can unambiguously incorporate $q\bar{q}$ bound state effects, and we expect that this approach can provide a fundamental underpinning to many processes described by effective meson lagrangians.

Acknowledgments: I would like to thank Peter Tandy for our collaboration on the electromagnetic form factors; the work on π - π scattering was done in collaboration with Pedro Bicudo, Steve Cotanch, Felipe Llanes-Estrada, Emilio Ribiero, and Adam Szczepaniak; I would also like to thank Dennis Jarecke, Chueng-Ryong Ji, and Craig Roberts for useful discussions. This work was funded by DOE under grants No. DE-FG02-96ER40947 and DE-FG02-97ER41048, and by NSF under grant No. INT-9807009, and benefitted from the resources of the National Energy Research Scientific Computing Center.

References

- [1] C. D. Roberts and S. M. Schmidt, Prog. Part. Nucl. Phys. **45S1**, 1 (2000); R. Alkofer and L. von Smekal, Phys. Rept. **353**, 281 (2001); see also M.B. Hecht and C.D. Roberts, arXiv:nucl-th/0110058, these proceedings.
- [2] P. Maris and C. D. Roberts, Phys. Rev. C **56**, 3369 (1997).
- [3] P. Maris and P. C. Tandy, Phys. Rev. C **60**, 055214 (1999).
- [4] P. Maris and P. C. Tandy, Phys. Rev. C **61**, 045202 (2000).
- [5] P. Maris and P. C. Tandy, Phys. Rev. C **62**, 055204 (2000).
- [6] Particle Data Group, C. Caso *et al.*, Eur. Phys. J. **C3**, 1 (1998).
- [7] S. R. Amendolia *et al.* [NA7 Collaboration], Nucl. Phys. B **277**, 168 (1986).
- [8] P. Brauel *et al.*, Z. Phys. C **3**, 101 (1979).
- [9] J. Volmer *et al.* [The Jefferson Lab F(π) Collaboration], Phys. Rev. Lett. **86**, 1713 (2001).
- [10] S. R. Amendolia *et al.*, Phys. Lett. B **178**, 435 (1986).
- [11] W. R. Molzon *et al.*, Phys. Rev. Lett. **41**, 1213 (1978) [Erratum-ibid. **41**, 1523 (1978)].
- [12] P. Maris and C. D. Roberts, Phys. Rev. C **58**, 3659 (1998).
- [13] C. Ji and P. Maris, Phys. Rev. D **64**, 014032 (2001).
- [14] A. Apostolakis *et al.*, Phys. Lett. **B473**, 186 (2000).
- [15] P. C. Tandy, Prog. Part. Nucl. Phys. **39**, 117 (1997).
- [16] J. W. Van Orden, N. Devine and F. Gross, Phys. Rev. Lett. **75**, 4369 (1995).
- [17] M. B. Hecht, C. D. Roberts and S. M. Schmidt, arXiv:nucl-th/0106011.
- [18] P. Maris and P. C. Tandy, arXiv:nucl-th/0109035.
- [19] D. Jarecke, P. Maris, and P.C. Tandy, in preparation.
- [20] S. Weinberg, Phys. Rev. Lett. **17**, 616 (1966).
- [21] P. Bicudo, S. Cotanch, F. Llanes-Estrada, P. Maris, E. Ribeiro and A. Szczepaniak, arXiv:hep-ph/0112015.
- [22] G. Colangelo, J. Gasser and H. Leutwyler, Phys. Lett. B **488**, 261 (2000).